jove

Neuroimaging-Guided TMS–EEG for Real-Time Cortical Network Mapping

Elena Ukharova[1], **Sabin Sathyan**[1], **Ida Granö**[1], **Isabella O'Meeghan**[1], **Oskari Ahola**[1,2,3], **Noora Kainulainen**[1], **Joonas Laurinoja**[1,4], **Paula Partanen**[5,6], **Dogu Baran Aydogan**[1,4], **Risto J. Ilmoniemi**[1], **Timo Roine**[1], **Pantelis Lioumis**[1,7,8]

[1] Department of Neuroscience and Biomedical Engineering, Aalto University School of Science [2] Hertie-Insitute for Clinical Brain Research, University of Tübingen [3] Department of Neurology and Stroke, University of Tübingen [4] A.I. Virtanen Institute for Molecular Sciences, University of Eastern Finland [5] Division of Psychology, VISE, Faculty of Education and Psychology, University of Oulu [6] Neuroscience Center, Helsinki Institute of Life Science, University of Helsinki [7] BioMag Laboratory, HUS Medical Imaging Center, Aalto University, University of Helsinki and Helsinki University Hospital [8] Cognitive Brain Research Unit, Department of Psychology and Logopedics, Faculty of Medicine, University of Helsinki

Corresponding Author

Elena Ukharova
elena.ukharova@aalto.fi

Citation

Ukharova, E., Sathyan, S., Granö, I., O'Meeghan, I., Ahola, O., Kainulainen, N., Laurinoja, J., Partanen, P., Aydogan, D.B., Ilmoniemi, R.J., Roine, T., Lioumis, P. Neuroimaging-Guided TMS–EEG for Real-Time Cortical Network Mapping. *J. Vis. Exp.* (220), e67339, doi:10.3791/67339 (2025).

Date Published

June 13, 2025

DOI

10.3791/67339

URL

jove.com/video/67339

Abstract

The cerebral cortex is organized into structurally and functionally segregated networks, enabling the human brain to process information highly efficiently. Transcranial magnetic stimulation (TMS), in combination with electroencephalography (EEG), offers a non-invasive approach to probing brain networks, revealing cortical excitability and causal connectivity. However, this method faces two significant challenges: (a) ensuring the quality of TMS-evoked potentials (TEPs) to maximize information gain, often requiring comprehensive cortical mapping, and (b) eliciting the response from the network of interest and not from adjacent cortical sites.

Existing TMS targeting approaches frequently fail to precisely stimulate functionally relevant cortical areas, hindering treatment efficacy and the identification of biomarkers. The presented protocol integrates precise cortical mapping to acquire artifact-free TEPs, enabling reliable and reproducible measurements of early TEP components. This precision improves sensitivity to subtle neurophysiological variations and strengthens correlations with clinical phenotypes, supporting biomarker discovery in neuropsychiatric disorders.

The proposed protocol utilizes structural, functional, and diffusion magnetic resonance imaging (MRI) to identify cortical patches belonging to the network of interest. Anatomical parcellation, functional connectivity, and real-time tractography are applied to locate areas with strong connectivity to other brain regions associated with the target network. The resulting personalized cortical clusters define the initial stimulation targets.

TMS–EEG mapping is then employed to optimize TMS parameters by localizing cortical areas with high excitability, enhancing neuronal response magnitude while reducing non-neuronal noise, including muscle artifacts, decay, and other confounding factors affecting early TMS–EEG responses. A systematic exploration of the cortical mantle is conducted, adjusting stimulation location, orientation, and intensity, with continuous data quality monitoring through real-time visualization of averaged TEPs. TMS parameters producing artifact-free responses with clearly discernible early TEP components are selected for data collection.

This article introduces the neuroimaging-guided TMS–EEG mapping technique and highlights the methodological advancements and benefits achievable through its application.

Introduction

The human brain is characterized by distinct large-scale structural and functional networks. The intricate interactions within and between the networks enable the brain's remarkable information-processing power, supporting complex cognitive, sensory, and motor processes. Disruptions in these networks, whether due to structural damage, functional dysregulation, or impaired connectivity, can lead to a wide range of neurological and psychiatric conditions[1,2,3,4,5,6], including motor deficits, cognitive impairments, and mood disorders. Accurately monitoring the progression of such network-related disorders and identifying optimal treatment strategies require methods that can selectively perturb specific networks and reliably quantify their functional integrity.

Transcranial magnetic stimulation, when delivered efficiently, can non-invasively perturbs neuronal populations and even entire cortical networks[7,8,9,10,11,12,13,14,15], allowing their assessment through measures such as motor responses or behavioral changes. TMS in combination with electroencephalography (EEG) allows one to measure TMS-evoked potentials (TEPs) – trial-averaged EEG responses time-locked to the TMS pulse. TEP waveforms recorded beneath the coil capture the immediate cortical excitability of the stimulated area, while responses from distant regions provide insights into effective connectivity between brain areas, establishing TMS–EEG as a valuable tool for investigating cortical networks. TEPs have already shown significant potential as biomarkers for various neurological[9,16,17] and psychiatric conditions[18,19,20,21,22,23]. Moreover, concurrent TMS–EEG allows for personalized stimulation intensities to be decided based on the local cortical reactivity of the individual as measured by EEG[24,25,26,27,28]. However, the challenge of this method, especially when used for biomarker development[22,24], is two-fold: a) to maximize information gain, the quality of the collected TEPs must be high, requiring mapping of the cortical areas to locate a target with minimal artifacts and good reactivity, and b) the response has to come from the network of interest and not from adjacent cortical sites. Low TEP quality is a common

issue, often manifesting as noise, artifacts, multisensory responses, or early responses that fail to exceed the power of ongoing oscillatory activity. This poor signal quality is typically identified only after offline processing, often long after data collection, making it difficult or impossible to address.

Navigated TMS (nTMS)[29], utilizing structural magnetic resonance imaging to target specific brain areas, has been available for clinical practice and research for more than 20 years. It has been crucial in mapping motor and speech cortical areas for presurgical evaluation[30,31,32] and for targeting areas that do not involve motor, visual, or behavioral responses by combining it with EEG[9,33,34,35]. However, it can be unspecific neuroanatomically (*i.e.*, the borders between cortical regions are not clear) and functionally, as individual variability in brain function cannot be detected using structural MRI. As such, current TMS targeting approaches, commonly reliant on the location of the motor cortex or other anatomical landmarks, often fail to stimulate functionally relevant cortical areas, limiting both treatment efficacy and the discovery of reliable biomarkers. To overcome these challenges, a comprehensive framework has been developed that integrates the use of other MRI modalities, such as functional and diffusion MRI, with precise cortical mapping for artifact-free TEP acquisition. This approach enables reliable and reproducible measurements, particularly of early TEP components, which are highly sensitive to subtle neurophysiological changes. By enhancing the sensitivity of TEP analysis, this framework facilitates robust correlations with clinical phenotypes, establishing a strong foundation for biomarker exploration in neuropsychiatric disorders.

The proposed pipeline is designed to map entire cortical areas, combining anatomical parcellation[36] (**Figure 1A**), functional MRI (fMRI)-based functional connectivity[37,38] (**Figure 1B**), and real-time tractography[39] (**Figure 1C**). Anatomical parcellation allows the delineation of cortical areas corresponding to a specific brain network for an individual, using a predefined anatomical template or brain atlas nonlinearly registered to individual brain anatomy. Functional connectivity provides statistical metrics that measure the correlation between the physiological activity of different brain regions, as reflected by the blood-oxygen-level-dependent (BOLD) signal[40]. Lastly, real-time tractography is a method based on diffusion MRI (dMRI) that estimates and displays streamlines describing potential structural brain connections in real-time. With the combination of these methods, cortical areas can be targeted based on their structural and functional connectivity during the TMS–EEG mapping. This enables the refinement of stimulation parameters in real-time to ensure artifact-free TEP acquisition.

The proposed novel methodology addresses the combined challenges of TMS targeting and TEP acquisition, paving the way for more precise biomarker identification and effective neuromodulation strategies in clinical and research settings.

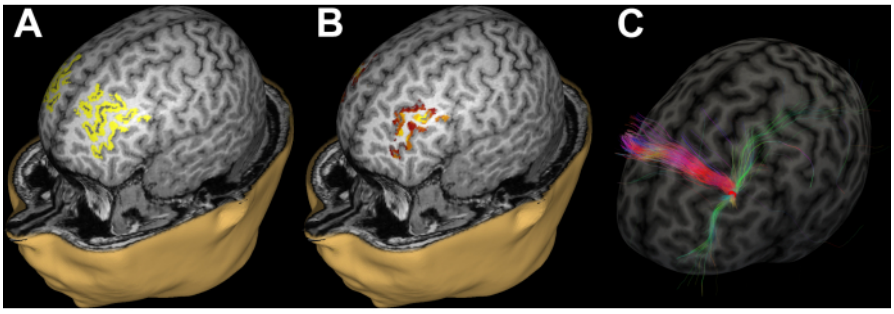

Figure 1: MRI-derived information for a representative subject. (**A**) Anatomical parcellation outlining the targeted dorsolateral prefrontal cortex (DLPFC). (**B**) Functional connectivity map showing anti-correlation with the subgenual cingulate cortex (lighter colors indicate stronger anti-correlation). (**C**) Real-time tractography displaying streamlines seeded from the targeted area. Please click here to view a larger version of this figure.

Protocol

This study was approved by the Hospital District of Helsinki and Uusimaa ethics committee. Prior to the procedure, written informed consent to participate was obtained from each subject.

1. Hardware and software requirements

1. Requirements for the experimental setup
    1. Ensure that the EEG system is TMS-compatible and is capable of recording at the sampling frequency of 5000 Hz or higher.
    2. Equip the EEG cap with at least 60 Ag/AgCl-sintered C-shaped or other electrodes that minimize induction of eddy currents by the TMS pulse[28].
    NOTE: The proposed protocol requires the use of passive electrodes. Although active electrodes are less sensitive to impedance levels, they are susceptible to decay artifacts[28], which can obscure early TEP components.
    3. Confirm whether the EMG system has a built-in algorithm for motor threshold determination. If not, the 10–20 approach should be used (see step 3.5.5.)
    4. Allow jittering of the TMS interstimulus interval within the range of 2–2.4 s minimum.
    5. Set the TMS recharge timing to be sufficiently delayed after the TMS pulse (e.g., 900–1000 ms post-pulse) to ensure the recharge artifact does not contaminate the time window of interest.
    6. Ensure the online neuronavigation system supports the import of overlays into anatomical images.
    NOTE: While external software can be used to visualize overlays and manually transfer coordinates to the neuronavigation system, this approach increases the complexity of the setup and extends the experiment duration.

7. Acquire specialized audiometric insert earphones for noise masking.

2. Software requirements

1. For the real-time visualization of TEPs during the experiment, install rt-TEP[25] (https://github.com/iTCf/rt-TEP), a MATLAB-based tool that nearly instantaneously plots streamed EEG data, averaging it around the TMS pulse.

NOTE: Some EEG systems allow the creation of similar visualizations directly within acquisition software. Ensure that the tool is reliable and allows minimal data manipulations such as cut-off of the TMS artifact and filtering-the success of the experiment relies heavily on online visualization.

2. Install the real-time tractogram visualizer (https://github.com/baranaydogan/realTimeTractogramVisualizer)[39] on a Linux PC to allow real-time visualization of the tracts.

3. Install the noise masking[41] (www.github.com/iTCf/TAAC).

4. For the MRI analysis, install the following software packages (or their alternatives): FreeSurfer[42], fmriprep[43], MRtrix3[44], as well as a Python environment with the nilearn library (https://nilearn.github.io).

2. Preparation of MRI-based priors for TMS targeting

1. Selection of regions of interest

1. Select at least two regions of interest (ROIs): one as the TMS target cortical area to be stimulated and another as the seed theorized to contribute significantly to the studied brain network. Use structural and functional connections from the seed to the target to refine the TMS target definition.

NOTE: While the TMS target must be accessible for stimulation, the seed can be any brain region, including deep gray matter areas like the amygdala.

2. MRI acquisition

1. Acquire a high-resolution anatomical T_1-weighted (T1w) magnetization-prepared rapid acquisition gradient echo (MPRAGE) image with 1-mm isotropic voxels.

2. Run echo-planar imaging (EPI) protocol to record 10 min of the fMRI BOLD signal in a resting state. Instruct the subject to keep their eyes open and fixated on a cross displayed on the screen for the duration of the sequence.

3. Apply the EPI protocol for dMRI, acquiring images in at least 100 different gradient directions total *(b* = 1500 and 3000 s/mm^2) and 12 non-diffusion-weighted (*b* = 0 s/mm^2) volumes with anterior-posterior phase-encodingdirection.

1. Acquire at least 1 additional unweighted volume with the reverse phase-encoding direction (posterior-anterior).

2. To improve tolerance for distortions caused, for instance, by subject motion, acquire several non-diffusion-weighted images in the reverse phase-encoding direction. In addition, repeating the full acquisition in reverse phase-encoding direction may be useful for new correction methods[45,46].

3. Anatomical MRI analysis

1. Preprocess the T1w image using FreeSurfer's[42] **recon-all** command. Visually inspect the brain mask (*brain.mgz*) and pial surfaces (*lh.pial* and *rh.pial*) to ensure proper removal of the dura. If neural tissue is excluded or the pial surface includes non-neural tissue, rerun **recon-all** with adjusted watershed parameters. Use the -**wsthresh** option to set the threshold value (default: 25, range: 0–50), or use -**wsmore** to expand or -**wsless** to shrink the brain mask.

2. With Human Connectome Project multi-modal parcellation 1.0[36] projected onto FreeSurfer's *fsaverage* surface (https://figshare.com/articles/dataset/HCP-MMP1_0_projected_on_fsaverage/3498446?file=5528837), resample the project parcellation to the brain surface of the subject using **mri_surf2surf**. With **mri_aparc2aseg**, create volumetric parcellation of the subject's cortical and subcortical regions. To align the parcellation with the original T1w image, run **mri_label2vol**, using *rawavg.mgz* as a template.

3. Select ROI parcels using the HCPMMP 1.0 look-up table and extract structural ROI maps from the volumetric parcellation in the subject's native space using **mri_binarize**.
   NOTE: If the seed ROI is defined by MNI coordinates from the literature rather than anatomical location, use a transformation matrix to map the coordinates from MNI to the subject's native space. Create a spherical ROI at the resulting location using a tool like the FSL function **fslmaths -kernel sphere**.

4. Functional MRI analysis

1. Preprocess BOLD data with fmriprep[43]. It can be done before the anatomical MRI analysis as fmriprep default settings call for **recon-all** or, alternatively, provide ready FreeSurfer output to the pipeline.
   NOTE: To speed up the preprocessing, restrict the analysis to the subject-specific space by passing the **--output-spaces T1w** flag to fmriprep. In this case, fmriprep will not perform the coregistration and consequent analysis in the MNI space.

2. Follow the steps below to perform whole brain seed-to-voxel analysis with preferred tools, e.g., using Python and nilearn library. The resulting volumetric maps quantify the temporal correlation between the BOLD signal in the seed and the rest of the brain.

3. Unless certain that the MR scanner includes dummy scans at the beginning of the sequence that is not recorded, remove the first 4 to 6 time points from the data. This will ensure that the data do not include the period of signal stabilization at the beginning of the recording.
   NOTE: For nilearn, use **.slicer** method, calling ***img*.slicer[…, 4:]**, where *img* is the imported functional MRI.

4. To denoise, use the confounds estimated by fmriprep. Among the confounds, select ones corresponding to head motion (*trans_x*, *trans_y*, *trans_z*, *rot_x*, *rot_y*, *rot_z*), average signal within the brain (*global_signal*), white matter (*white_matter*), and cerebrospinal fluid (*csf*). Use selected values as nuisance regressors in a general linear model to remove non-neural parts of the signal.

5. Reduce the false positives with 0.01–0.08 Hz band-pass filtering. if using nilearn, perform confound regression and filtering with **nilearn.image.clean_img** by passing the confound matrix and cut-off frequencies to the function.
6. Smooth the data with a 6-mm Full Width Half Maximum (FWHM) Gaussian kernel. Pass **smoothing_fwhm=6** parameter to **nilearn.maskers.NiftiMasker** to smooth the image.
7. Extract and average the time series from the seed mask. Apply seed ROI mask with **nilearn.maskers.NiftiMasker** to extract time series from the functional data.
8. Calculate the Pearson correlation coefficient between the averaged time series of the seed and every other voxel within the brain mask. Convert the resulting correlation coefficients to Fisher's *z*-score to transform the correlation coefficients to a normal distribution.
   NOTE: To compute the correlation, take the dot product between the brain and ROI time series using **np.dot** and divide it by the time series length. Apply np.arctanh to convert the resulting coefficients to Fisher's z-score.
9. Restrict the resulting map to the ROIs by multiplying the correlation map with the ROI masks, *e.g.,* by using **nilearn.image.math_img**. The resulting images will keep the correlation values within the voxels of the mask and zeros elsewhere.
10. Optionally, threshold the maps, e.g., to include only negatively correlated voxels. Use **nilearn.image.threshold_img** with the corresponding threshold parameter.

5. Diffusion MRI analysis
   1. Preprocess diffusion data with a pipeline including denoising[47], correction for motion[48], susceptibility-induced distortions[49], Gibbs ringing[50,51], and eddy current artifacts[52]. Generate a fiber orientation density (FOD) map and a brain mask.
      NOTE: The DESIGNER toolbox (https://nyu-diffusionmri.github.io/DESIGNER-v2/) offers a fully automated preprocessing pipeline. FOD estimation can be performed using **dwi2response dhollander** and **dwi2fod msmt_csd**[53,54,55] commands from the MRtrix3[44] toolbox (https://www.mrtrix.org/). Ensure that FOD and brain masks are coregistered to T1 space to match with the neuronavigation system. Ensure that gradient or FOD orientations are rotated during the coregistration[56,57]. Use of MRtrix3 command **mrregister** is recommended.
   2. Use **mri_label2vol** command to move FreeSurfer's aparc+aseg.mgz segmentation to the native MRI space. Then run ***aparc+aseg_to_trekkerACTlabels.py*** (https://raw.githubusercontent.com/dmritrekker/trekker/master/extensions/tools/aparc%2Baseg_to_trekkerACTlabels.py) on the segmentation in the original MRI space to create anatomically constrained tractography (ACT) file.
   3. Upload T1, brain mask, FOD, and ACT files to the real-time tractogram visualizer (see step 1.2.2.) and carefully confirm that the visualized tracts look viable[58].

3. TMS–EEG experiment

1. EEG preparation

    1. Ensure the abrasive and conductive gels do not contain metallic components that may induce decay artifacts.

    2. Seat the subject in a chair positioned close enough for the cap cables to connect to the EEG system while leaving space around them for unrestricted movement.

        NOTE: It is possible to do the EEG preparation with the subject sitting in the TMS chair. However, the chair's headrest and overall bulk might make access to the subject's head more difficult, making the process more time-consuming.

    3. Start EEG preparation by measuring the subject's head circumference. Select a matching size of the EEG cap.

        NOTE: If the head circumference falls between cap sizes, choose the smaller size, as a loose fit may create gaps between the electrodes and the scalp.

    4. Put the cap on, starting from the forehead, keeping the hair under the cap. When the cap is roughly in place, measure the distances from nasion to inion and from left to right tragus. Adjust the cap position, making sure that Cz is placed halfway between the anatomical landmarks.

    5. Prepare the ground and reference electrodes by cleaning the mastoid and zygomatic bone skin opposite to the stimulation side with alcohol wipes and abrasive tape to improve conductivity. Place the ground electrode on the zygomatic bone and the reference on the mastoid using ring electrode washers.

        NOTE: Electrode placement varies across labs (see Hernandez-Pavon et al., 2023[28]). While Cz is often used as a reference, it may be suboptimal due to proximity to the coil. Mastoid and zygomatic placements or positions on the forehead below the cap are recommended, depending on the distance from the stimulation target and the neuronavigation setup.

    6. Prepare the ground and reference electrodes. Apply an abrasive paste first and lightly scrub the skin under the electrodes with a blunt needle or with a cotton bud. Then, fill the electrode with conductive gel.

    7. Fix the cap in place using hook-and-loop fasteners under the chin. Make sure that the ear slits are located correctly, allowing access to the ears for the neuronavigation and placing earphones for the noise masking.

    8. Prepare the cap electrodes in a similar manner as ground and reference. First, add a small amount of abrasive gel and use the blunt needle or wooden end of a cotton swab stick to remove the hair under the electrode so the skin is visible.

    9. Fill the electrode with conductive gel while gently pressing the electrode down to ensure that the amount of gel is sufficient but not excessive. Keep the impedance of every electrode for the TMS–EEG experiment under 5 kΩ.

        NOTE: While the amount of conductive gel has to be sufficient to create a connection between the scalp

and the electrode, excessive amounts may lead to bridging between neighboring electrodes.

10. If the impedance is higher than that after the initial preparation, use a blunt needle or cotton swab again and swirl it inside the electrode to further scrub the skin. Try to avoid getting hair out of the electrode. Fill the fixed electrode with conductive gel again and check the impedance. Repeat the process until all electrodes are below 5 kΩ.

2. EMG preparation

    1. Clean each electrode site with alcohol wipes, lightly scratching the skin with abrasive tape, wipe again with alcohol, and allow it to dry. Place the active electrode on the muscle belly (commonly the right abductor pollicis brevis (APB) and/or first dorsal interosseous (FDI)), the reference electrode over the muscle tendon, and the ground electrode on the dorsum of the hand.

3. Neuronavigation preparation

    1. Place the subject in the chair in a comfortable position, ensuring they are seated comfortably with the neck, hands, and legs relaxed. Adjust the chair height to allow the operator to comfortably stimulate the entire area under investigation.

    2. Secure the head tracker using a medical grade two-sided sticker or tape to ensure it remains stable during the stimulation session. Position the sticker so that it does not obstruct the free movement of the TMS coil over the head.

        NOTE: Position the tracker slightly to the right on the forehead when stimulating the left hemisphere and slightly to the left when stimulating the right hemisphere. This arrangement facilitates access to the frontal lobe areas.

    3. Identify the cardinal points (nasion and preauricular points) on the subject's MRI.

        NOTE: When defining preauricular points, carefully check if the subject's ears were pressed during the MRI acquisition by the foam and ear protection. Opt for deeper parts of the ear lobe, such as the crus of the helix, which are not as prone to being deformed on MRI scans.

    4. Using a digitizing pen, mark the cardinal points on the subject's head corresponding to those identified on the MRI.

    5. Digitize additional points across the skull surface to minimize registration errors.

    6. Confirm that the registration error is below 3 mm (below 2 mm is preferable).

    7. Press the digitization pen to the subject's head in several locations and confirm that the corresponding points on the 3D head model look correct. If not, repeat the co-registration procedure.

4. Noise masking

    1. Prepare the noise masking[41] — looped audio recording of white noise with mixed-in coil clicks recorded from the utilized type of coil. Make sure that the noise masking is on only when TMS pulses are delivered to reduce the subject's discomfort.

    2. Use specialized air-tube earphones with earplug-like tips to mask the noise of the TMS click during the recording.

    3. Select the correct size of the ear tips and instruct the subject to squeeze them before placing them in the

ear canal. Visually confirm that the earphones are placed correctly.

4. Before starting, show the subject the raw EEG signal and demonstrate how facial muscle clenching, blinking, and eye movements create artifacts. Explain that these artifacts reduce data quality and adjust the subject's position for comfort to minimize muscle tension noise.

5. Instruct the subject to focus their eyes on the fixation cross located in front of them when TMS pulses are given.

6. Fix the coil several centimeters above the vertex. Select a high stimulation intensity that is unlikely to be needed for the experiment, e.g., 80% of MSO, to ensure that the noise level is high enough to suppress louder coil clicks.

7. Explain to the subject the nature of noise masking and that their task is to try to distinguish between coil clicks coming from the coil placed above their head and the clicks coming from the earphones as the volume level is increased. Instruct the subject to give a sign, such as lifting a thumb, when they believe they cannot hear the click coming from the TMS coil anymore.

8. Turn on the noise masking, starting with the default setting and changing the white noise-click ratio to 60%.

9. Start giving the pulses with a jittered interstimulus interval. Increase the volume on the PC with noise-masking 1%-2% at a time until the subject gives a sign that they cannot perceive the click anymore.

10. If the subject still can perceive the click, try to adjust the white noise-click ratio up (for the high-pitch component of the click) or down (for the low-pitch component). Consult Russo et al., 2022[41] for further instructions, if necessary.

    NOTE: If the auditory response is persistent, the earphone's placement should be checked — the ear tip's location might be too shallow.

11. Ensure that the volume of the noise masking does not exceed safety limits for the estimated duration of the experiment[41]. After the volume has been defined, ask the subject whether they experience the volume as tolerable for the duration of the experiment.

    NOTE: According to the US National Institute for Occupational Safety and Health (NIOSH)[59], a noise level of 88 dB can be safely tolerated for up to 4 h. For every 3 dB increase above this level, the permissible exposure time is halved, whereas for every 3 dB decrease, the permissible exposure time doubles.

12. Give 20 to 30 pulses while checking real-time TEP visualization. If there is a visible amplitude change within 100- to 200-ms latency after the pulse in electrodes under the coil and the temporal electrodes, it is likely to be the auditory response to the click (auditory evoked potential). Increase the masking noise volume in the 2% steps until this component disappears.

5. Determination of resting motor threshold (RMT)

    1. Instruct the subject to keep their muscles relaxed with the palm facing upwards.

    2. Confirm that the EMG signal noise (peak to peak) does not exceed 20 μV at rest, which otherwise can interfere with the determination of the size of the

motor evoked potential (MEP). If there is a persistent presence of noise, try to rearrange the position of the EMG cables, if applicable, or disconnect unnecessary electrical devices from the sockets, minimizing environmental noise.

3. Position the TMS coil over the motor knob with the electric field perpendicular to the sulcus. Begin with ~30% MSO, adjusting intensity until localized muscle activation is observed.

4. Keep the intensity and adjust the coil location and orientation over the motor knob until a target eliciting a muscle response[60, 61] specific to APB is found or another muscle of choice. Save the target location for the motor threshold determination.

5. Using the saved location, use either automated algorithms[62] to determine RMT or a 10–20 approach[60] — out of 20 pulses given with fixed intensity, 10 should produce MEP with amplitude over 50 µV. Increase or decrease stimulation intensity in steps of 1%–2% of MSO until the conditions are fulfilled. Save the intensity value for further use.

6. Cortical mapping

1. Overlay the anatomical parcellations and functional connectivity maps produced using MRI data in the neuronavigation software.

NOTE: Typically, only one overlay is available at a time. First overlay the anatomical parcellation map to understand the extent of the brain area and then switch to the functional connectivity map to identify smaller relevant subregions.

2. Investigate the locations with the strongest connectivity using real-time tractography. The optimal stimulation target must demonstrate either widespread structural connectivity[63,64] if the hypothesis does not prioritize particular white matter pathways or a significant number of streamlines leading towards other regions of the cortical network under investigation.

3. Define at least 2–3 targets that show promise in terms of functional and/or structural connectivity to be tested with TMS–EEG.

4. Place the coil over the area exhibiting the strongest functional connectivity properties with the posterior-anterior direction of the induced electric field.

5. Start giving TMS pulses at 100% to 110% of RMT over the selected location with the noise masking on. Average 20 pulses at a time and inspect the resulting TEPs. If there is a visible TEP response, increase or decrease the stimulation intensity in 2% MSO increments until the early TEP (15–50 ms latency) amplitude is bigger than 6 µV, 6–10 µV being the optimal range[25].

6. If a discernible TEP is not observed, gradually increase the stimulation intensity by 5% of the MSO until the TEP amplitude reaches the target threshold of 6 µV. Record the stimulation locations that generate promising TEP responses and return to these sites for further optimization.

7. Monitor the signal for muscle and decay artifacts. If muscle artifacts persist beyond 15 ms, first rotate the coil to minimize them. If unsuccessful, adjust the stimulation site medially and posteriorly while remaining within the structural region of interest, guided by MRI overlays.

NOTE: Optimization may not always eliminate artifacts over 15 ms, but improvements are possible. Ensure subject comfort, especially when stimulating frontal and temporal regions, where stimulation can be painful. Pain perception may not correlate with artifact size; in such cases, prioritize tolerability over optimal targeting to avoid increased muscle tension, sensory artifacts, and compromised data quality.

8. When the location and orientation producing muscle and decay artifact-free TEP with early components exceeding 6 µV is found, check the TEP for the presence of visible components past 50 ms. If TEP components are absent, increase stimulation intensity in 2% MSO increments. If the intensity increase does not produce the needed result, shift the stimulation target to the next one defined in step 3.6.3.

9. When multiple potential stimulation targets are identified, evaluate each one carefully using real-time tractography. Achieve this by either copying the location coordinates from the neuronavigation system or identifying the target using anatomical landmarks. Prioritize targets that, when applicable, demonstrate direct connections to the regions of interest (as outlined in step 2.1.1) or exhibit higher global structural connectivity.

10. When the location and orientation producing the most prominent response to TMS are found, save the information about them to start the recording.

7. TMS–EEG data recording

1. Before beginning each data recording, measure the electrode impedances. If any electrodes have an impedance higher than 5 kΩ, add a small amount of conductive gel to lower the impedance, as it may increase throughout the experiment due to drying. If this adjustment is insufficient, repeat the EEG preparation process, adding more gel only if necessary.

2. Confirm that the subject cannot hear the coil clicks and inquire about any pain or discomfort. Encourage the subject to stretch before finding a comfortable position, then reiterate instructions on maintaining eye fixation.

NOTE: Given the long experiment duration, include short breaks between mapping and recording sessions. Offer water and assess the subject's comfort and tolerance of the process. Breaks also help prevent drowsiness. Adjust the chair position if needed and recheck electrode impedances after each break.

3. Collect at least 300 trials with the noise masking using the stimulation location, orientation, and intensity finalized in step 3.6.10. The interstimulus interval may vary but must have the jitter and exceed 2 s.

NOTE: The number of pulses depends on the aims and needs of each study[28].

4. Carefully digitize the electrode locations with the neuronavigation system for the consequent data analysis.

Representative Results

The described protocol was used to collect TMS–EEG data from the left dorsolateral prefrontal cortex (DLPFC) of a healthy volunteer. The study was approved by The Coordinating Ethics Committee of Helsinki University Hospital and carried out in accordance with the Declaration of Helsinki.

The subject signed an informed consent form. For the data acquisition details, refer to **Table of Materials**.

Left DLPFC is a common area of interest, used in clinical practice for repetitive TMS treatment of major depressive disorder (MDD)[65]. A growing body of literature highlights the importance of the functional connectivity of the subgenual anterior cingulate cortex (sgACC) with DLPFC in the pathophysiology of MDD[3,66,67]. In particular, there are indications that the TMS treatment delivered over the areas of the left DLPFC showing strong anti-correlation with the left sgACC might have higher efficacy[38,68,69,70]. Following these findings, it is hypothesized that TMS–EEG data recorded from the targets functionally anticorrelated with sgACC BOLD activity is going to be most informative for further biomarker development.

The structural MRI mask for DLPFC was defined as a combination of the regions 9a, 9p, 9-46d, 46, a9-46v, and p9-46v from the HCPMMP[36], encompassing Brodmann areas 9 and 46. The sgACC mask was region 25, equivalent to Brodmann area 25. Following the described protocol, seed-to-voxel correlation maps were derived using fMRI data and selected only voxels belonging to the DLPFC ROI. The maps were then thresholded to only display voxels with negative correlation; the absolute value of the correlation was taken to simplify the visualization. The resulting clusters were overlaid on the structural MRI in the neuronavigation during the TMS–EEG experiment (**Figure 2A**).

The initial TMS–EEG mapping targets were selected from regions that exhibited the strongest functional anticorrelation with the sgACC. These targets were then iteratively refined through the TMS–EEG mapping procedure to identify the most promising stimulation sites based on TEP quality and their proximity to cortical patches with the highest anticorrelation to the sgACC. The finalized set of potential stimulation sites was subsequently analyzed using real-time tractography. Since there is no known direct pathway from the sgACC to the DLPFC, indirect white matter pathways had to be considered. In cases where specific direct or indirect pathways are known a priori, these should be prioritized. For the sgACC, the large-scale brain network affected by MDD[3] was taken into account during the tractography-driven target selection. The structural connectivity of the TMS target was also evaluated, with areas showing broad connectivity to other brain regions — such as the ventromedial prefrontal cortex, Broca's area, or the parietal lobe — being given higher priority.

Following the mapping protocol, the target, orientation, and intensity of the stimulation were chosen based on the resulting TEPs being larger than 6 µV and minimally affected by artifacts. Each optimization iteration involved recording 20 pulses with minimal preprocessing. The final optimized target was then used to collect 300 pulses for data analysis.

The minimal preprocessing pipeline, designed to simulate real-time rt-TEP use, involved the following steps:

1. Division of data into epochs
2. Baseline correction
3. Removal of the TMS artifact by replacing data from -2 to 10 ms around TMS pulse by zeros
4. Removal of the bad channels
5. Re-referencing to the average reference
6. A low-pass filter at 80 Hz and a notch filter at 48–52 Hz were applied when necessary to address line and high-frequency noise.

The full preprocessing pipeline followed the procedures outlined in Mutanen et al., 2024[71]. For further details on TMS–EEG preprocessing, refer to Hernandez-Pavon et al.,

2022[72], Rogasch et al., 2017[73], Mutanen et al., 2018[74], and Mutanen et al., 2016[75]. In summary, the process included:

1. Division of data into epochs
2. Baseline correction
3. TMS artifact removal between -2 and 10 ms around the TMS pulse, with cubic interpolation using 5 ms of data before and after the removed interval
4. Removal of bad channels (4 in total: Fpz, F1, FT10, TP9, PO4)
5. Removal of bad trials
6. Removal of drifts with robust detrending
7. ICA for removal of ocular artifacts
8. Baseline correction
9. Application of the SOUND[74] algorithm to suppress extracranial noise, followed by re-referencing to the average reference
10. SSP-SIR[75] algorithm to remove TMS-evoked muscle artifacts
11. Low-pass filtering at 80 Hz and a notch filter at 48–52 Hz
12. Snipping the ends of the time window to remove possible edge effects
13. Additional removal of bad trials to ensure residual high-noise trials are excluded (22 out of 300 rejections total)

The experimental procedure started with the identification of the resting motor threshold. Subject's RMT was 41% MSO.

During the experimental procedure, primarily the electrodes over the region of interest (AF3, F1, F3, F5, FC3) (**Figure 2B**) were examined to assess the quality of the resulting TEPs. Other electrodes were continuously monitored for low impedance, and the impedance was lowered as needed, following the procedure outlined in step 3.1.10. The early TMS responses within the 10 to 60 ms time window, which reflect the direct activation of the cortex by the induced electric field, were used to evaluate the quality of the produced TEPs.

The mapping procedure (see **Figure 3**) began with one of the fMRI clusters (**Figure 3A**) and an investigation of the structural connectivity of the target area (**Figure 3B**), which primarily showed streamlines to the homologous area in the contralateral hemisphere and frontal pole.

For the stimulation, the coil was oriented at 45 degrees to the midline. The stimulation intensity was set at 49% MSO, corresponding to 96 V/m estimated E-field maximum at the hotspot and 120% RMT. In **Figure 3C**, a potential TEP-like response is observed in the F3, F1, and FC3 electrodes. The AF3 electrode exhibits a large-amplitude ringing artifact, while F5 is affected by a small muscle artifact recognizable by the high-frequency high-amplitude peak right after the TMS pulse[76,77]. To minimize the ringing artifact during recording, a net cap pressing the electrodes down to reduce movement or a thin foam layer beneath the coil can be used (see Hernandez-Pavon et al., 2023[28]). Although such artifacts can often be removed through filtering, since only AF3 was contaminated, it was excluded from the average reference to avoid unnecessary filtering, resulting in the data shown in **Figure 3D**.

Focusing on the F3 electrode (**Figure 3F**), the signal appears largely unaffected by the muscle artifact observed in F5. The characteristic large-amplitude waveform recovers around 15 ms, and a 5-microvolt deflection between 22 ms and 32 ms is likely a genuine cortical response to TMS. Filtering the signal (**Figure 3E**, **G**) confirms that the amplitude remains unaffected by noise in other channels.

To investigate whether the muscle artifact in the F5 channel could be reduced through coil rotation, all other stimulation

parameters were kept constant (**Figure 4**), and the coil was first rotated to a posterior-anterior orientation (**Figure 4A**), where the E-field maximum was estimated to be 80 V/m and then to a lateral-medial direction (**Figure 4E**), with 101 V/m E-field maximum. A sharp increase in muscle activation was observed with the posterior-anterior coil orientation (**Figure 4B**,**C**), which was reported as uncomfortable by the subject. The lateral-medial orientation produced a signal similar to the one shown in **Figure 3**, but with a larger amplitude, resulting in an early 12 µV TEP response at the F3 electrode (**Figure 4F**,**G**), which allows a reduction in stimulation intensity. The lack of excessive muscle, decay, or ringing artifacts, along with the size of the early TEP response, makes this combination of stimulation parameters a promising candidate for the data collection.

Figure 5 shows the effect of stimulation intensity on TEP responses in low-excitability target. The second fMRI cluster (**Figure 5A**) and its structural connectivity (**Figure 5B**) were then investigated. Similarly to the first target, the structural connections seem to be limited to the frontal lobes. It is noteworthy that despite the distance between the two fMRI clusters being 28 mm, the stimulation intensity used for the previous targets, 49% MSO (77 V/m, 120% RMT), produced no discernible TMS response, highlighting the importance of TEP-based selection of stimulation intensity. In **Figure 5B,C**, the TMS response at 55% MSO (89 V/m, 134% RMT) is shown. It is important to note that the large deflection observed after 10 ms is not a genuine TMS response but rather a continuation of the muscle artifact recovery. Therefore, only signals occurring later than 25 ms after the pulse should be considered, resulting in an amplitude of 4 µV between 26 ms and 60 ms. The intensity was further increased to 60% MSO (97 V/m, 146% RMT) in an attempt to obtain distinct earlier responses (**Figure 5F**,**G**). Compared to the 55% MSO intensity, an expected increase in the amplitude of the muscle artifact was observed, but there was little to no increase in the TEP amplitude. Based on the observed waveform and the need for a higher stimulation intensity, this target would be considered to exhibit lower cortical excitability compared to the previous targets, making it less informative for data collection. However, a target with similar properties might be preferable for treatment protocols.

In total, 16 distinct combinations of stimulation parameters were investigated using a 20-trial mapping procedure. The total duration of the procedure, excluding the EEG and EMG preparation (which took approximately 30 min), was 2 h 35 min. The final stimulation target can be seen in **Figure 6A**. While being very close to the initial target (**Figure 3A**), this target exhibits much more widespread structural connectivity (**Figure 6B**), potentially providing more information on the signal propagation from the hotspot to other cortical regions. The stimulation intensity was kept at 49% MSO (102 V/m, 120% RMT).

The minimal preprocessing of the first 20 pulses collected from the final stimulation target is shown in **Figure 6C**,**D.** Large amplitude ringing contaminated the F1 electrode, which was subsequently rejected. However, residual noise remained present in other electrodes even after this rejection. Despite the presence of the ringing artifact, the absence of the muscle artifact within the region of interest allowed for considering the latencies after 16 ms as a genuine neural signal. After filtering, the amplitude of the early component between 17 ms and 35 ms was 9 µV.

Figure 6E,**F** show the result of the full preprocessing pipeline applied to the 300-pulse dataset. The resulting TEP closely resembles the waveform derived from 20 pulses (**Figure 6D**), demonstrating the relevance of real-time monitoring of the

TEPs. The early response between 20 ms and 40 ms is 6 μV, demonstrating the expected reduction in amplitude due to the preprocessing.

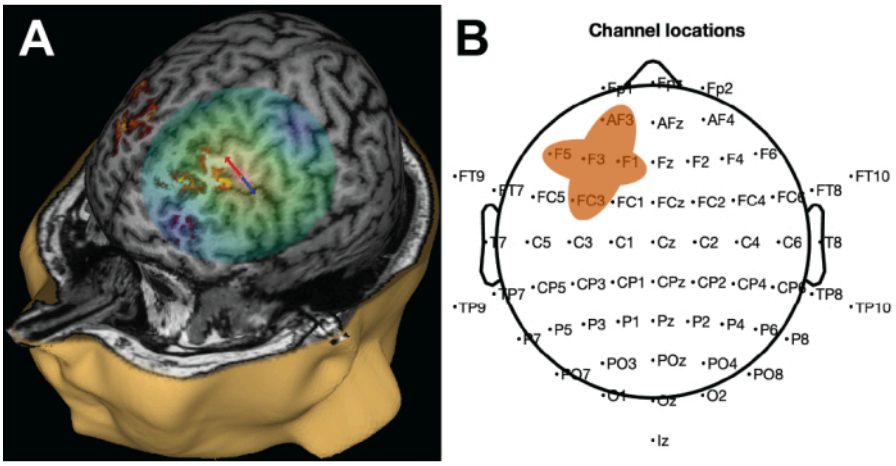

Figure 2: Neuronavigation and electrode setup. (**A**) Subject's 3D MRI-based head model overlaid with fMRI-derived connectivity. (**B**) Schematic of EEG electrode placement, with electrodes of interest under the stimulation coil marked in orange. Note that the locations of the electrodes are digitized on the 3D head model (step 3.7.4). Please click here to view a larger version of this figure.

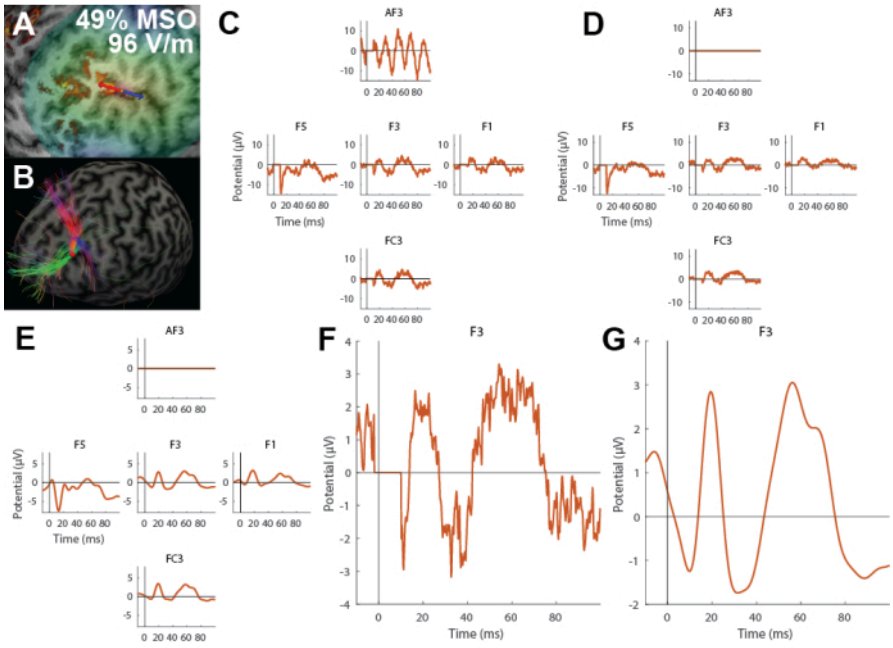

Figure 3: An example of minimal TMS–EEG data processing. (**A**) The neuronavigation display shows the stimulation site and coil orientation. The red arrow indicates the stronger direction of the biphasic pulse, and the blue arrow indicates the weaker direction. Stimulation intensity is expressed as a percentage of maximum stimulator output (MSO) and resting motor threshold (RMT). (**B**) Real-time tractography at the stimulation location. (**C**) Raw TMS–EEG data from electrodes beneath the stimulation coil. (**D**) TMS–EEG data after noisy channel rejection, with rejected channels replaced by zeros. (**E**) TMS–EEG data after filtering. (**F**) Zoomed-in view of the F3 electrode after bad channel rejection. (**G**) Zoomed-in view of the F3 electrode after filtering. Please click here to view a larger version of this figure.

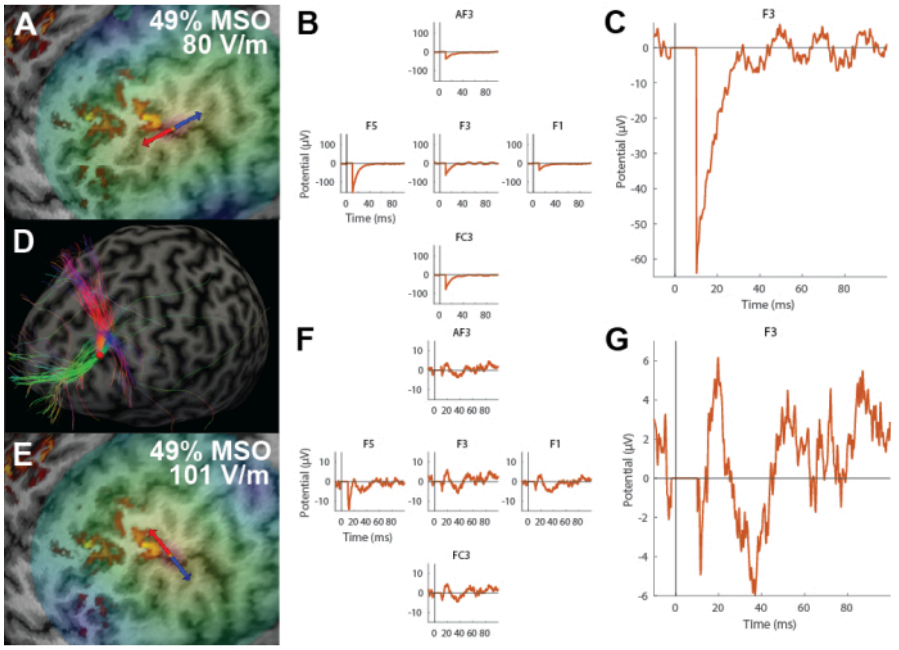

Figure 4: Effect of stimulation orientation on the muscle artifact. (**A**) Stimulation target with posterior-anterior coil orientation and corresponding intensity. (**B**) Raw data for posterior-anterior orientation, showing muscle artifact contamination. (**C**) Data from F3 electrode with large muscle artifact. (**D**) Real-time tractography corresponding to the stimulation location. (**E**) Stimulation target with lateral-medial orientation and corresponding intensity. (**F**) Raw data for lateral-medial orientation, showing clean TEPs. (**G**) TEP from the F3 electrode, exhibiting a large, artifact-free early response. Please click here to view a larger version of this figure.

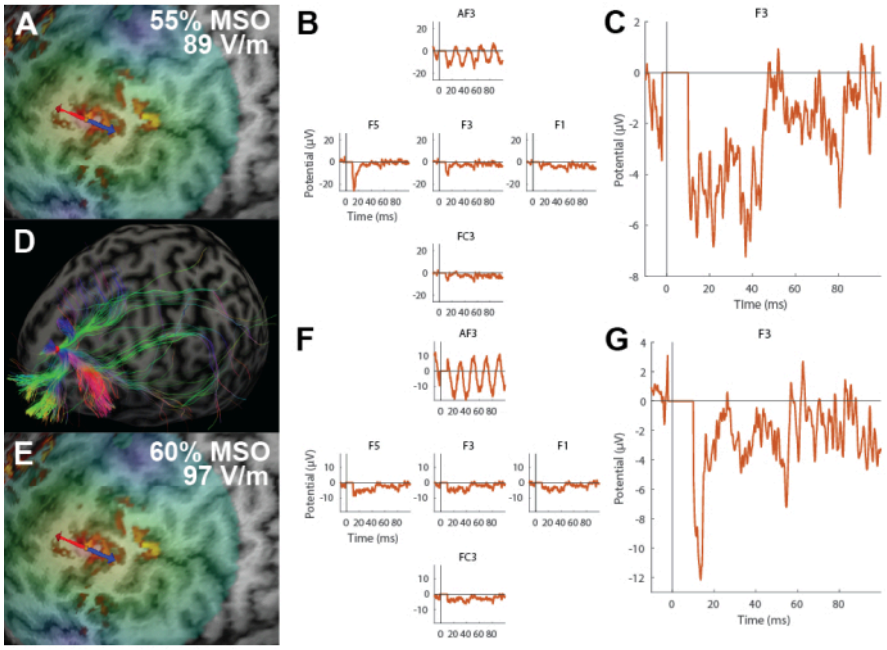

Figure 5: Effect of stimulation intensity on TEP responses in low-excitability target. (**A**) Stimulation target location and intensity. (**B**) Raw data recorded at 55% MSO. C) F3 electrode data, lacking distinguishable early TEP components. (**D**) Real-time tractography corresponding to the stimulation location. (**E**) Stimulation intensity increased while keeping the target constant. (**F**) Raw data recorded at 60% MSO. (**G**) F3 electrode data showing muscle artifacts due to higher stimulation intensity. Please click here to view a larger version of this figure.

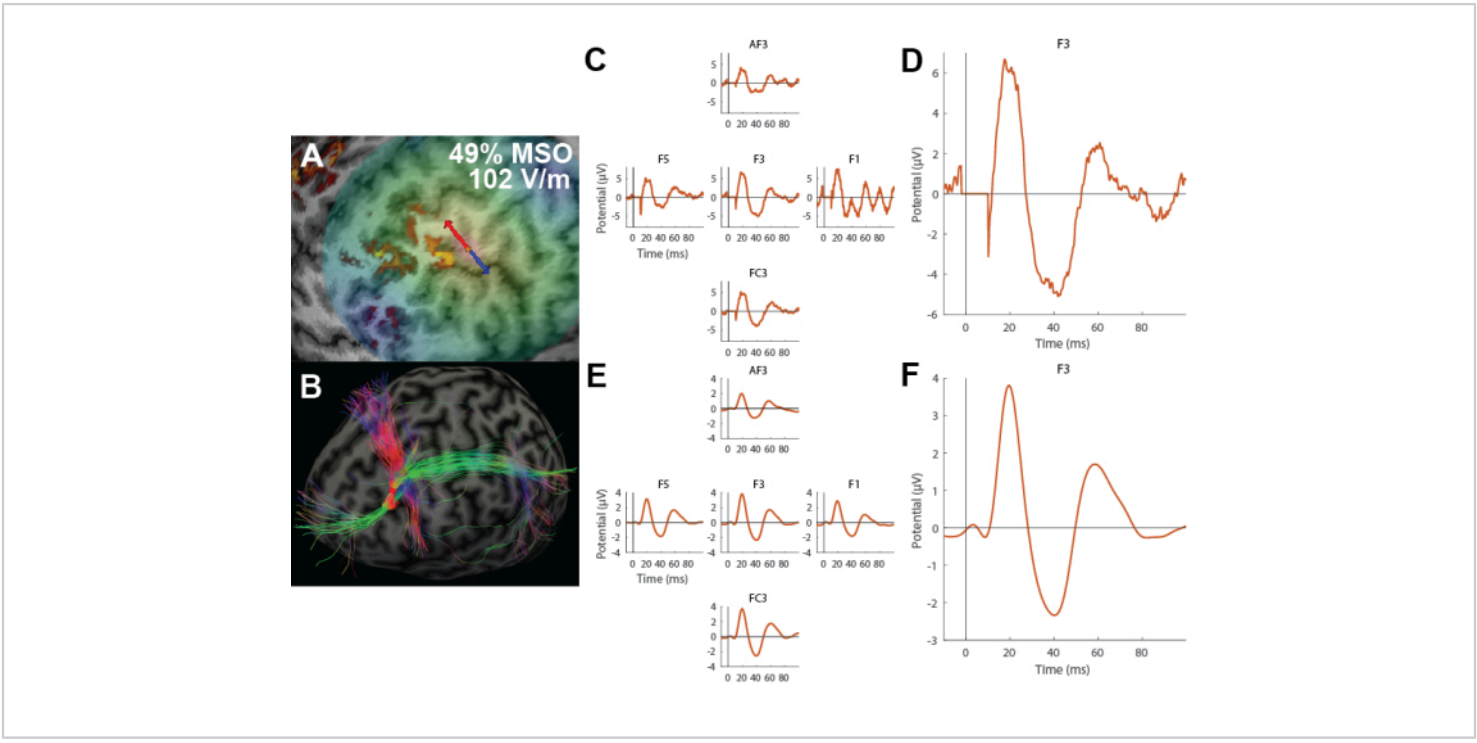

Figure 6: Effect of minimal and full preprocessing pipelines on the TMS–EEG data. (**A**) Final stimulation target and intensity. (**B**) Real-time tractography for the stimulation location. (**C**) Raw data averaged over 20 trials. (**D**) 20-trial average TEP at the F3 electrode. (**E**) Fully preprocessed TEPs averaged over 300 trials. (**F**) Fully preprocessed 300-trial average TEP at the F3 electrode. Please click here to view a larger version of this figure.

Discussion

This methodological pipeline introduces a novel approach for personalized brain mapping and targeting using multiple neuroimaging techniques. Individualized cortical maps are constructed by combining anatomical parcellation with functional and structural connectivity, which helps define the initial search region for the optimal stimulation target. Next, TMS–EEG mapping is employed to refine the target's location, orientation, and stimulation intensity, aiming to enhance the reactivity of early neuronal responses to TMS and reduce muscle, decay, and other artifacts. Cortical areas within the region of interest are systematically explored, adjusting the stimulation location, electric-field orientation, and intensity, while data quality is continuously monitored through real-time visualization of averaged TEPs. The final stimulation target is selected based on artifact-free responses with clearly identifiable early TEP components. This pipeline is especially useful for studies focused on exploring TMS-EEG-based biomarkers.

The pipeline consists of several essential and demanding steps. The first step involves defining the cortical area boundaries for TMS–EEG mapping. Without this, the target may be selected from an area with a different cytoarchitecture than the functionally relevant one. To address this, the Human Connectome Project multimodal parcellation[36] is utilized, which divides brain regions based on a combination of structural and functional connectivity. The derived mask

defines the outer boundaries of the area to be mapped with TMS–EEG. To further refine the cortical area of interest (e.g., DLPFC, a rather large brain region), voxels demonstrating functional connectivity to the sgACC (area 25)[38,68,78], recently incorporated into clinical practices for MDD treatment[69,79], are selected. From there, TMS–EEG mapping begins by targeting cortical regions with the strongest functional connectivity to the sgACC, ensuring the selected area exhibits high cortical reactivity without contamination from muscle or decay artifacts. If raw TEPs recorded after 20 pulses meet quality standards, the target is chosen for data collection. However, if significant artifacts are observed — a frequent issue in the prefrontal cortex — adjacent regions are systematically explored to identify a suitable alternative.

Real-time tractography may help in selecting TMS targets with large-scale structural connectivity, such as the spatially distributed networks implicated in MDD[3,78], which are not limited to a single white matter tract. However, it is particularly valuable in cases involving known tracts, like the frontal aslant tract in the speech network, where it ensures precise targeting[80]. Although offline tractography can provide connectivity information that is useful for ROI selection, it is less effective for TMS–EEG mapping. Predefined cortical targets identified through offline methods may fail to elicit relevant or sufficiently strong EEG responses, may not effectively engage the desired network, or could result in discomfort and muscle artifacts, compromising data quality and necessitating parameter adjustments during the experiment. By dynamically offering connectivity insights, real-time tractography addresses these challenges, allowing for on-the-fly optimization of coil placement to ensure high-quality, reliable measurements and robust network engagement.

In this protocol, the intensity of TMS is adjusted based on EEG signals reflecting cortico-cortical excitability, while using RMT primarily as a starting point for intensity calibration. RMT plays a secondary role in determining the final intensity. This approach ensures the activation of a significant population of neurons within the target area, producing a strong and reliable signal. Once artifacts are minimized through coil adjustments and functional and structural validation of the target, stimulation intensity is further adjusted. Since this protocol aims to maximize the data obtained from TMS–EEG responses for biomarker identification, it is crucial to ensure that TEP amplitudes are adequate. When using RMT to define intensity, early responses typically do not exceed 4 μV[81] after preprocessing, which, combined with artifacts, reduces the quality of the neural signal. To overcome this, an approach developed by Casarotto et al.[25] and refined by Tervo et al.[82] is used, involving averaging the EEG signal in real-time after 20–30 TMS pulses. The goal is to achieve a clear, non-artifactual response of 6–10 μV in a 10–50 ms window. As shown in Figures 3 and 5, closely located targets may require different stimulation intensities, leading to either insufficient or excessive neuronal activation.

Standard non-navigated targets, typically defined using distances from the motor hotspot or the 10–20 EEG system electrode locations, are widely used in rTMS treatments[83,84,85,86]. They have also been effective in TMS–EEG studies targeting the DLPFC, with biomarkers like later responses (e.g., N100) and long-interval intracortical inhibition (LICI) showing potential[18,19,23,87,88]. These non-personalized targets are simpler, cost-effective, and do not require MRI, neuronavigation, or specialized personnel

for target identification, and some have been shown to reliably locate the DLPFC[85,86]. However, the lack of personalization may contribute to lower remission rates in treatments[89,90]. Moreover, cranial muscles in the area may obscure early responses due to artifacts that prevent intensity adjustment. Personalized intensity adjustments in TMS may therefore improve treatment effectiveness.

This protocol advances a more personalized approach to brain stimulation that provides better insight into cortical reactivity and connectivity compared to standard non-personalized approaches. However, it demands substantial resources, including individual MRI scans, specialized TMS and EEG equipment, and personnel with expertise in neuroimaging and neurophysiology. Moreover, the proposed approach heavily depends on the subjective judgment of the TEP quality and optimal stimulation parameters. Despite these limitations, the quality of the TMS–EEG data is critical for biomarker development, justifying the use of this approach. Once reliable biomarkers are identified, the procedure may be simplified to focus on optimizing relevant time windows and minimizing artifacts. In the future, as TMS technology advances (e.g., multi-locus[91] and multi-channel[92] TMS), the resource requirements for personalized stimulation are expected to decrease, potentially making it the new standard for clinical use.

Disclosures

PL is a consultant to Nexstim Plc for TMS–EEG applications and speech cortical mapping. RI has patents on TMS technology and has consulted Nexstim Plc on TMS.

Acknowledgments

xWe would like to thank Profs. Silvia Casarotto, Marcello Massimini, and Mario Rosanova from the University of Milan for pioneering and promoting TMS–EEG mapping methodology. We also would like to acknowledge the contribution of the dozens of research participants that led to the development of our experimental protocol. Work on "PlaStim: Plasticity Stimulation in the Treatment of Anhedonia" is supported by Wellcome Leap as part of the Multi-Channel Psych Program. This project has also received funding from the European Research Council (ERC) under the European Union's Horizon 2020 Research and Innovation Programme (grant agreement No 81037).

References

1. Fornito, A., Zalesky, A., Breakspear, M. The connectomics of brain disorders. *Nat Rev Neurosci.* **16** (3), 159-172 (2015).
2. Stam, C. J. Hub overload and failure as a final common pathway in neurological brain network disorders. *Netw Neurosci.* **8** (1), 1-23 (2024).
3. Siddiqi, S. H. et al. Brain stimulation and brain lesions converge on common causal circuits in neuropsychiatric disease. *Nat Hum Behav.* **5** (12), 1707-1716 (2021).
4. Xu, M. et al. Reconfiguration of structural and functional connectivity coupling in patient subgroups with adolescent depression. *JAMA Netw Open.* **7** (3), e241933 (2024).
5. Fields, R. D. White matter in learning, cognition and psychiatric disorders. *Trends Neurosci.* **31** (7), 361-370 (2008).
6. van den Heuvel, M. P., Sporns, O. A cross-disorder connectome landscape of brain dysconnectivity. *Nat Rev Neurosci.* **20** (7), 435-446 (2019).

7. Momi, D. et al. Networklevel macroscale structural connectivity predicts propagation of transcranial magnetic stimulation. *NeuroImage.* **229**, 117698 (2021).
8. Ozdemir, R. A. et al. Individualized perturbation of the human connectome reveals reproducible biomarkers of network dynamics relevant to cognition. *Proc Natl Acad Sci U S A.* **117** (14), 8115-8125 (2020).
9. Massimini, M., Ferrarelli, F., Huber, R., Esser, S. K., Singh, H., Tononi, G. Breakdown of cortical effective connectivity during sleep. *Science.* **309** (5744), 2228-2232 (2005).
10. Bortoletto, M., Veniero, D., Thut, G., Miniussi, C. The contribution of TMS–EEG coregistration in the exploration of the human cortical connectome. *Neurosci Biobehav Rev.* **49**, 114-124 (2015).
11. Rogasch, N. C., Fitzgerald, P. B. Assessing cortical network properties using TMS-EEG. *Hum Brain Mapp.* **34** (7), 1652-1669 (2013).
12. MüllerDahlhaus, F., Bergmann, T. O. Network perturbationbased biomarkers of depression and treatment response. *Cell Rep Med.* **4** (6), 101086 (2023).
13. Bergmann, T. O., Varatheeswaran, R., Hanlon, C. A., Madsen, K. H., Thielscher, A., Siebner, H. R. Concurrent TMSfMRI for causal network perturbation and proof of target engagement. *NeuroImage.* **237**, 118093 (2021).
14. Casali, A. G., Casarotto, S., Rosanova, M., Mariotti, M., Massimini, M. General indices to characterize the electrical response of the cerebral cortex to TMS. *NeuroImage.* **49** (2), 1459-1468 (2010).
15. Solomon, E. A. et al. TMS provokes targetdependent intracranial rhythms across human cortical and subcortical sites. *Brain Stimul.* **17** (3), 698-712 (2024).
16. Comolatti, R. et al. A fast and general method to empirically estimate the complexity of brain responses to transcranial and intracranial stimulations. *Brain Stimul.* **12** (5), 1280-1289 (2019).
17. Casarotto, S. et al. Stratification of unresponsive patients by an independently validated index of brain complexity. *Ann Neurol.* **80** (5), 718-729 (2016).
18. Dhami, P. et al. Prefrontal cortical reactivity and connectivity markers distinguish youth depression from healthy youth. *Cereb Cortex.* **30** (7), 3884-3894 (2020).
19. Dhami, P. et al. Neurophysiological markers of response to theta burst stimulation in youth depression. *Depress Anxiety.* **38** (2), 172-184 (2021).
20. Hadas, I., Hadar, A., Lazarovits, A., Daskalakis, Z. J., Zangen, A. Right prefrontal activation predicts ADHD and its severity: A TMS–EEG study in young adults. *Prog Neuropsychopharmacol Biol Psychiatry.* **111**, 110340 (2021).
21. Hoy, K. E., Coyle, H., Gainsford, K., Hill, A. T., Bailey, N. W., Fitzgerald, P. B. Investigating neurophysiological markers of impaired cognition in schizophrenia. *Schizophr Res.* **233**, 34-43 (2021).
22. Kallioniemi, E., Daskalakis, Z. J. Identifying novel biomarkers with TMS–EEG – methodological possibilities and challenges. *J Neurosci Methods.* **377**, 109631 (2022).
23. Sun, Y. et al. Indicators for remission of suicidal ideation following magnetic seizure therapy in patients with treatmentresistant depression. *JAMA Psychiatry.* **73** (4), 337-345 (2016).

24. Lioumis, P., Rosanova, M. The role of neuronavigation in TMS-EEG studies: Current applications and future perspectives. *J Neurosci Methods.* **380**, 109677 (2022).
25. Casarotto, S. et al. The rtTEP tool: realtime visualization of TMSevoked potentials to maximize cortical activation and minimize artifacts. *J Neurosci Methods.* **370**, 109486 (2022).
26. Koch, G. et al. Precuneus magnetic stimulation for Alzheimer's disease: A randomized, shamcontrolled trial. *Brain.* **145** (11), 3776-3786 (2022).
27. Casula, E. P. et al. Regional precuneus cortical hyperexcitability in Alzheimer's disease patients. *Ann Neurol.* **93** (2), 371-383 (2023).
28. HernandezPavon, J. C. et al. TMS combined with EEG: Recommendations and open issues for data collection and analysis. *Brain Stimul.* **16** (2), 567-593 (2023).
29. Hannula, H., Ilmoniemi, R. J. Basic principles of navigated TMS. *Navigated Transcranial Magnetic Stimulation in Neurosurgery.* 3-29. (2017).
30. Vitikainen, A.M. et al. Combined use of noninvasive techniques for improved functional localization for a selected group of epilepsy surgery candidates. *NeuroImage.* **45** (2), 342-348 (2009).
31. Krieg, S. M. et al. Protocol for motor and language mapping by navigated TMS in patients and healthy volunteers; workshop report. *Acta Neurochirurgica.* **159** (7), 1187-1195 (2017).
32. Lioumis, P. et al. A novel approach for documenting naming errors induced by navigated transcranial magnetic stimulation. *J Neurosci Methods.* **204** (2), 349-354 (2012).
33. Lioumis, P., Kicić, D., Savolainen, P., Mäkelä, J. P., Kähkönen, S. Reproducibility of TMSevoked EEG responses. *Hum Brain Mapp.* **30** (4), 1387-1396 (2009).
34. Rosanova, M., Casali, A., Bellina, V., Resta, F., Mariotti, M., Massimini, M. Natural frequencies of human corticothalamic circuits. *J Neurosci.* **29** (24), 7679-7685 (2009).
35. Harquel, S., Bacle, T., Beynel, L., Marendaz, C., Chauvin, A., David, O. Mapping dynamical properties of cortical microcircuits using robotized TMS and EEG: Towards functional cytoarchitectonics. *NeuroImage.* **135**, 115-124 (2016).
36. Glasser, M. F. et al. A multimodal parcellation of human cerebral cortex. *Nature.* **536** (7615), 171-178 (2016).
37. Cash, R. F. H., Zalesky, A. Personalized and circuitbased transcranial magnetic stimulation: Evidence, controversies, and opportunities. *Biol Psychiatry.* **95** (6), 510-522 (2024).
38. Fox, M. D., Liu, H., PascualLeone, A. Identification of reproducible individualized targets for treatment of depression with TMS based on intrinsic connectivity. *NeuroImage.* **66**, 151-160 (2013).
39. Aydogan, D. B. et al. Realtime tractographyassisted neuronavigation for TMS. *bioRxiv.* (2023).
40. van den Heuvel, M. P., Hulshoff Pol, H. E. Exploring the brain network: A review on restingstate fMRI functional connectivity. *Eur Neuropsychopharmacol.* **20** (8), 519-534 (2010).
41. Russo, S. et al. TAAC-TMS adaptable auditory control: A universal tool to mask TMS clicks. *J Neurosci Methods.* **370**, 109491 (2022).

42. Fischl, B. FreeSurfer. *NeuroImage.* **62** (2), 774-781 (2012).

43. Esteban, O. et al. fMRIPrep: A robust preprocessing pipeline for functional MRI. *Nat Methods.* **16** (1), 111-116 (2019).

44. Tournier, J.D. et al. MRtrix3: A fast, flexible and open software framework for medical image processing and visualisation. *NeuroImage.* **202**, 116137 (2019).

45. Qiao, Y., Shi, Y. Unsupervised deep learning for FODbased susceptibility distortion correction in diffusion MRI. *IEEE Trans Med Imaging.* **41** (5), 1165-1175 (2022).

46. Irfanoglu, M. O., Modi, P., Nayak, A., Hutchinson, E. B., Sarlls, J., Pierpaoli, C. DRBUDDI (Diffeomorphic Registration for BlipUp blipDown Diffusion Imaging) method for correcting echo planar imaging distortions. *NeuroImage.* **106**, 284-299 (2015).

47. Veraart, J., Novikov, D. S., Christiaens, D., AdesAron, B., Sijbers, J., Fieremans, E. Denoising of diffusion MRI using random matrix theory. *NeuroImage.* **142**, 394-406 (2016).

48. Leemans, A., Jones, D. K. The Bmatrix must be rotated when correcting for subject motion in DTI data. *Magn Reson Med.* **61** (6), 1336-1349 (2009).

49. Andersson, J. L. R., Skare, S., Ashburner, J. How to correct susceptibility distortions in spinecho echoplanar images: Application to diffusion tensor imaging. *NeuroImage.* **20** (2), 870-888 (2003).

50. Kellner, E., Dhital, B., Kiselev, V. G., Reisert, M. Gibbsringing artifact removal based on local subvoxelshifts. *Magn Reson Med.* **76** (5), 1574-1581 (2016).

51. Lee, H.H., Novikov, D. S., Fieremans, E. Removal of partial Fourierinduced Gibbs (RPG) ringing artifacts in MRI. *Magn Reson Med.* **86** (5), 2733-2750 (2021).

52. Andersson, J. L. R., Sotiropoulos, S. N. An integrated approach to correction for offresonance effects and subject movement in diffusion MR imaging. *NeuroImage.* **125**, 1063-1078 (2016).

53. Tournier, J.D., Calamante, F., Connelly, A. Robust determination of the fibre orientation distribution in diffusion MRI: Nonnegativity constrained superresolved spherical deconvolution. *NeuroImage.* **35** (4), 1459-1472 (2007).

54. Dhollander, T., Raffelt, D., Connelly, A. Unsupervised 3tissue response function estimation from singleshell or multishell diffusion MR data without a coregistered T1 image. *Proc ISMRM Workshop Breaking Barriers Diffus MRI.* 5 (2016).

55. Jeurissen, B., Tournier, J.D., Dhollander, T., Connelly, A., Sijbers, J. Multitissue constrained spherical deconvolution for improved analysis of multishell diffusion MRI data. *NeuroImage.* **103**, 411-426 (2014).

56. Raffelt, D., Tournier, J.D., Crozier, S., Connelly, A., Salvado, O. Reorientation of fiber orientation distributions using apodized point spread functions. *Magn Reson Med.* **67** (3), 844-855 (2012).

57. Raffelt, D., Tournier, J.D., Fripp, J., Crozier, S., Connelly, A., Salvado, O. Symmetric diffeomorphic registration of fibre orientation distributions. *NeuroImage.* **56** (3), 1171-1180 (2011).

58. Schilling, K. G. et al. Limits to anatomical accuracy of diffusion tractography using modern approaches. *NeuroImage.* **185**, 1-11 (2019).

59. CDC. Noise and hearing loss. *Noise Hearing Loss.* .https://www.cdc.gov/niosh/noise/about/noise.html (2024).

60. Rossini, P. M. et al. Noninvasive electrical and magnetic stimulation of the brain, spinal cord, roots and peripheral nerves: Basic principles and procedures for routine clinical and research application. *Clin Neurophysiol.* **126** (6), 1071-1107 (2015).

61. Rothwell, J. C., Hallett, M., Berardelli, A., Eisen, A., Rossini, P., Paulus, W. Magnetic stimulation: motor evoked potentials. *Electroencephalogr Clin Neurophysiol Suppl.* **52**, 97-103 (1999).

62. Awiszus, F. TMS and threshold hunting. *Suppl Clin Neurophysiol.* **56**, 13-23 (2003).

63. Seguin, C., Jedynak, M., David, O., Mansour, S., Sporns, O., Zalesky, A. Communication dynamics in the human connectome shape the cortexwide propagation of direct electrical stimulation. *Neuron.* **111** (9), 1391-1401.e5 (2023).

64. Momi, D., Wang, Z., Griffiths, J. D. TMSevoked responses are driven by recurrent largescale network dynamics. *eLife.* **12**, e83232 (2023).

65. Fitzgerald, P. B. Targeting repetitive transcranial magnetic stimulation in depression: Do we really know what we are stimulating and how best to do it? *Brain Stimul.* **14** (3), 730-736 (2021).

66. Connolly, C. G. et al. Restingstate functional connectivity of subgenual anterior cingulate cortex in depressed adolescents. *Biol Psychiatry.* **74** (12), 898-907 (2013).

67. Schmaal, L. et al. Cortical abnormalities in adults and adolescents with major depression based on brain scans from 20 cohorts worldwide in the ENIGMA Major Depressive Disorder Working Group. *Mol Psychiatry.* **22** (6), 900-909 (2017).

68. Cash, R. F. H., Cocchi, L., Lv, J., Wu, Y., Fitzgerald, P. B., Zalesky, A. Personalized connectivityguided DLPFCTMS for depression: Advancing computational feasibility, precision and reproducibility. *Hum Brain Mapp.* **42** (13), 4155-4172 (2021).

69. Cole, E. J. et al. Stanford accelerated intelligent neuromodulation therapy for treatmentresistant depression. *Am J Psychiatry.* **177** (8), 716-726 (2020).

70. Hadas, I. et al. Association of repetitive transcranial magnetic stimulation treatment with subgenual cingulate hyperactivity in patients with major depressive disorder. *JAMA Netw Open.* **2** (6), e195578 (2019).

71. Mutanen, T. P., Ilmoniemi, I., Atti, I., Metsomaa, J., Ilmoniemi, R. J. A simulation study: comparing independent component analysis and signalspace projection-sourceinformed reconstruction for rejecting muscle artifacts evoked by transcranial magnetic stimulation. *Front Hum Neurosci.* **18**, 1324956 (2024).

72. HernandezPavon, J. C., Kugiumtzis, D., Zrenner, C., Kimiskidis, V. K., Metsomaa, J. Removing artifacts from TMSevoked EEG: A methods review and a unifying theoretical framework. *J Neurosci Methods.* **376**, 109591 (2022).

73. Rogasch, N. C. et al. Analysing concurrent transcranial magnetic stimulation and electroencephalographic data: A review and introduction to the opensource TESA software. *NeuroImage.* **147**, 934-951 (2017).

74. Mutanen, T. P., Metsomaa, J., Liljander, S., Ilmoniemi, R. J. Automatic and robust noise suppression in EEG and MEG: The SOUND algorithm. *NeuroImage.* **166**, 135-151 (2018).

75. Mutanen, T. P., Kukkonen, M., Nieminen, J. O., Stenroos, M., Sarvas, J., Ilmoniemi, R. J. Recovering TMSevoked EEG responses masked by muscle artifacts. *NeuroImage.* **139**, 157-166 (2016).

76. Mutanen, T., Mäki, H., Ilmoniemi, R. J. The effect of stimulus parameters on TMS-EEG muscle artifacts. *Brain Stimul.* **6** (3), 371-376 (2013).

77. Rogasch, N. C., Thomson, R. H., Daskalakis, Z. J., Fitzgerald, P. B. Shortlatency artifacts associated with concurrent TMS-EEG. *Brain Stimul.* **6** (6), 868-876 (2013).

78. Siddiqi, S. H., Weigand, A., PascualLeone, A., Fox, M. D. Identification of personalized transcranial magnetic stimulation targets based on subgenual cingulate connectivity: An independent replication. *Biol Psychiatry.* **90** (10), e55-e56 (2021).

79. Williams, N. R. et al. Highdose spaced thetaburst TMS as a rapidacting antidepressant in highly refractory depression. *Brain.* **141** (3), e18 (2018).

80. Lioumis, P. et al. Study design for navigated repetitive transcranial magnetic stimulation for speech cortical mapping. *J Vis Exp.* (2023).

81. Lioumis, P., Zomorrodi, R., Hadas, I., Daskalakis, Z. J., Blumberger, D. M. Combined transcranial magnetic stimulation and electroencephalography of the dorsolateral prefrontal cortex. *J Vis Exp.* (2018).

82. Tervo, A. E. et al. Closedloop optimization of transcranial magnetic stimulation with electroencephalography feedback. *Brain Stimul.* **15** (2), 523-531 (2022).

83. Trapp, N. T., Pace, B. D., Neisewander, B., Ten Eyck, P., Boes, A. D. A randomized trial comparing beam F3 and 5.5 cm targeting in rTMS treatment of depression demonstrates similar effectiveness. *Brain Stimul.* **16** (5), 1392-1400 (2023).

84. Fitzgerald, P. B., Maller, J. J., Hoy, K. E., Thomson, R., Daskalakis, Z. J. Exploring the optimal site for the localization of dorsolateral prefrontal cortex in brain stimulation experiments. *Brain Stimul.* **2** (4), 234-237 (2009).

85. Trapp, N. T. et al. Reliability of targeting methods in TMS for depression: Beam F3 vs. 5.5 cm. *Brain Stimul.* **13** (3), 578-581 (2020).

86. MirMoghtadaei, A. et al. Concordance between Beam F3 and MRIneuronavigated target sites for repetitive transcranial magnetic stimulation of the left dorsolateral prefrontal cortex. *Brain Stimul.* **8** (5), 965-973 (2015).

87. Sun, Y. et al. Magnetic seizure therapy reduces suicidal ideation and produces neuroplasticity in treatmentresistant depression. *Transl Psychiatry.* **8** (1), 253 (2018).

88. Hui, J. et al. Altered interhemispheric signal propagation in schizophrenia and depression. *Clin Neurophysiol.* **132** (7), 1604-1611 (2021).

89. Berlim, M. T., van den Eynde, F., TovarPerdomo, S., Daskalakis, Z. J. Response, remission and dropout rates following highfrequency repetitive transcranial magnetic stimulation (rTMS) for treating major depression: A systematic review and metaanalysis of randomized, doubleblind and shamcontrolled trials. *Psychol Med.* **44** (2), 225-239 (2014).

90. Fitzgerald, P. B., Hoy, K. E., Anderson, R. J., Daskalakis, Z. J. A study of the pattern of response to rTMS treatment in depression. *Depress Anxiety.* **33** (8), 746-753 (2016).

91. Nieminen, J. O. et al. Multilocus transcranial magnetic stimulation system for electronically targeted brain stimulation. *Brain Stimul.* **15** (1), 116-124 (2022).

92. Daneshszand, M., Navarro de Lara, L., Makarov, S., Meng, Q., Nummenmaa, A. A modular multichannel TMS system with threeaxis coil design. *Brain Stimul.* **16** (1), 134 (2023).